Nonequilibrium initial conditions from perturbative QCD for relativistic and ultrarelativistic heavy ion collisions

N. Hammon, H. Stöcker, and W. Greiner
Institut Für Theoretische Physik, Robert-Mayer Strasse 10, Johann Wolfgang Goethe-Universität, 60054 Frankfurt am Main, Germany
(Received 20 April 1999; published 24 November 1999)

We calculate the initial nonequilibrium conditions from perturbative QCD within Glauber multiple-scattering theory for $\sqrt{s}=200A$ GeV and $\sqrt{s}=5.5A$ TeV. At the soon available collider energies one will particularly test the small-x region of the parton distributions entering the cross sections. Therefore, shadowing effects, previously more or less unimportant, will lead to new effects on variables such as particle multiplicities dN/dy, transverse energy production $d\overline{E}_T/dy$, and the initial temperature T_i. In this paper we will take a closer look at the effects of shadowing by employing different parametrizations for the shadowing effect for valence quarks, sea quarks, and gluons. Since the cross sections at midrapidity are dominated by processes involving gluons the amount of their depletion is particularly important. We will therefore take a closer look at the results for dN/dy, $d\overline{E}_T/dy$, and T_i by using two different gluon shadowing ratios, differing strongly in size. As a matter of fact, the calculated quantities differ significantly.

PACS number(s): 25.75.−q, 12.38.Bx

I. INTRODUCTION

One of the challenging goals of heavy ion physics is the detection of the quark-gluon plasma, a state in which the partons are able to move freely within a distance larger than the typical confinement scale $r_{\mathrm{conf}}\sim 1/\Lambda_{\mathrm{QCD}}\sim 1/0.2$ GeV ~ 1 fm. The buildup of this state should happen early in a heavy ion reaction when the two streams of initially cold nuclear matter pass through each other. Thereby first virtual partons are transformed to real ones and later on in the expansion phase the fragmentation of the partons into colorless hadrons takes place. When separating perturbative QCD (pQCD) from nonperturbative effects at some semihard scale $p_0=2$ GeV the respective time scale of perturbative processes is thus of the order $\tau\sim 1/p_0\sim 0.1$ fm/c, which approximately coincides with the lower bound of the initial formation time of the plasma in a local cell [1]. Therefore, all further evolution of the system is significantly influenced by the initial conditions of pQCD since macroscopic parameters, such as, e.g., the initial temperature T_i, directly enter into hydrodynamical calculations.

We here will focus on the very early phase of an ultrarelativistic heavy ion collision and use pQCD above the semihard scale $p_{sh}=p_0=2$ GeV.

In a typical high-energy pp or $p\overline{p}$ event one measures distinct hadronic jets with a transverse momenta of several GeV ($p_T\geqslant 5$ GeV) [2]. In contrast to the experimental very clean situation of hadronic jets at large p_T one encounters the problem of detectability of low transverse momentum jets in heavy ion collisions. These so-called minijets contribute significantly to the transverse energy produced in AB collisions due to their large multiplicity [3]. The major part of these set-free partons are gluons that strongly dominate the processes as their number is much larger for the relevant momentum fractions. In turn the shadowing effects are expected to be much larger for gluons than for the quark sea [4]. Therefore, the relative contribution of the gluons should decrease but still dominate the cross sections. The shadowing of the gluons has the peculiarity of not being known exactly due to the neutrality of the mediators of the strong interaction which makes it impossible to access $R_G(x,Q^2)$ directly in a deep inelastic $e+A$ event. Therefore we will here investigate two possible parametrizations of the shadowing ratio $R_G=xG^A/A\cdot xG^N$ for gluons as will be described below in detail.

II. MINIJETS

As outlined above, we will here investigate the effects of shadowing on the minijet production cross sections. The production of a parton $f=g,q,\overline{q}$ can in leading order be described as [3]

$$\frac{d\sigma^f}{dy}=\int dp_T^2 dy_2 \sum_{ij,kl} x_1 f_i(x_1,Q^2) x_2 f_j(x_2,Q^2) \times\left[\delta_{fk}\frac{d\hat{\sigma}^{ij\to kl}}{d\hat{t}}(\hat{t},\hat{u})+\delta_{fl}\frac{d\hat{\sigma}^{ij\to kl}}{d\hat{t}}(\hat{u},\hat{t})\right]\frac{1}{1+\delta_{kl}}. \tag{1}$$

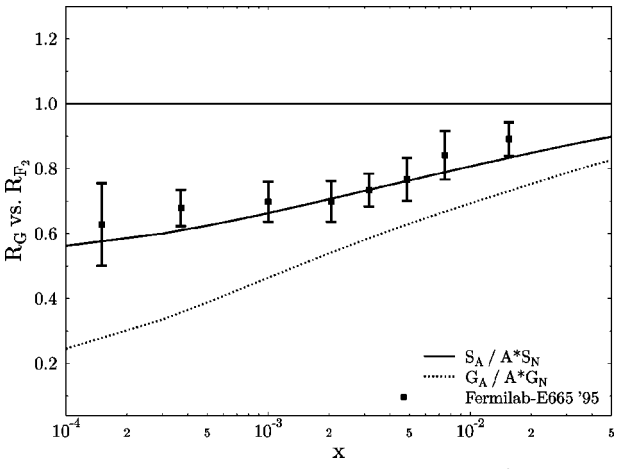

FIG. 1. R_{F_2} vs R_G at $Q^2=4$ GeV^2 for ^{207}Pb.

TABLE I. $\int dy\, dN^g/dy$ for $\sqrt{s}=200A$ GeV.

Range of y	$gg\to gg$	$gq\to gq + g\bar{q}\to g\bar{q}$	Total
All y	920.8	384.3	1305.1
$\lvert y\rvert\leq 0.5$	192.9	90.7	283.6

The factor $1/(1+\delta_{kl})$ enters due to the symmetry of processes with two identical partons in the final state. The exchange term $d\hat{\sigma}(\hat{t},\hat{u})\leftrightarrow d\hat{\sigma}(\hat{u},\hat{t})$ accounts for the possible symmetries of, e.g., having a quark from nucleon i and a gluon from nucleon j and vice versa, i.e., it handles the interchange of two of the propagators in the scattering process. The possible combinations of initial states are

$$ij=gg,gq,qg,g\bar{q},\bar{q}g,qq,q\bar{q},\bar{q}q,\bar{q}\bar{q}. \tag{2}$$

The momentum fractions of the partons in the initial state are

$$x_1=\frac{p_T}{\sqrt{s}}[e^{y}+e^{y_2}],\quad x_2=\frac{p_T}{\sqrt{s}}[e^{-y}+e^{-y_2}]. \tag{3}$$

The integration regions are

$$p_0^2\leq p_T^2\leq\left(\frac{\sqrt{s}}{2\cosh y}\right)^2,$$

$$-\ln\left(\frac{\sqrt{s}}{p_T}-e^{-y}\right)\leq y_2\leq\ln\left(\frac{\sqrt{s}}{p_T}-e^{-y}\right), \tag{4}$$

with

$$\lvert y\rvert\leq\ln\left(\frac{\sqrt{s}}{2p_0}+\sqrt{\frac{s}{4p_0^2}-1}\right). \tag{5}$$

The mandelstam variables are defined as

$$\hat{s}=x_1\cdot x_2\cdot s,\quad \hat{t}=-p_T^2[1+e^{(y_2-y)}],$$

$$\hat{u}=-p_T^2[1+e^{(y-y_2)}]. \tag{6}$$

For the parton distributions entering the handbag graph we choose the Glück, Reya, Vogt leading order set [5] for relativistic heavy ion collider (RHIC). Since at large hadron collider (LHC) one probes smaller momentum fractions we there use the newer CTEQ4L parametrization [6] with $N_f=4$ and $Q=p_T$. The normalization is done so that one has two outgoing partons in one collision, i.e.,

$$\int dy\,\frac{d\sigma^f}{dy}=2\sigma^f_{\rm hard}. \tag{7}$$

TABLE II. $\int dy\, dN^q/dy$ for $\sqrt{s}=200A$ GeV.

Range of y	$gq\to gq$	$qq\to qq$	$gg\to q\bar{q}$	$q\bar{q}\to q\bar{q}$	Total
All y	310.3	57.3	6.5	22.8	396.9
$\lvert y\rvert\leq 0.5$	21.0	7.4	1.5	2.3	32.2

TABLE III. $\int dy\, dN^{\bar{q}}/dy$ for $\sqrt{s}=200A$ GeV.

Range of y	$g\bar{q}\to g\bar{q}$	$q\bar{q}\to q\bar{q}$	$gg\to q\bar{q}$	$\bar{q}\bar{q}\to\bar{q}\bar{q}$	Total
All y	74.2	22.8	6.5	2.2	105.7
$\lvert y\rvert\leq 0.5$	12.5	5.3	1.5	0.4	19.7

In the calculations the boundaries for the calculations are either over the whole rapidity range or $\lvert y\rvert\leq 0.5$ for the central rapidity region.

To account for the higher-order contributions at RHIC we choose a fixed K factor of $K=2.5$ from comparison with experiment as discussed in [7,2]. In the range 5.5 GeV $\leq p_T\leq 25$ GeV a factor $K=2.5$ is needed to describe the UA1 data, and in the range 30 GeV$\leq p_T\leq 50$ GeV a factor of $K=1.6$ is needed. However, the cross section has dropped so much at these large transverse momenta that we keep $K=2.5$ fixed for all p_T. For LHC energies the mean p_T tends to be larger; so we choose $K=1.5$ for this case.

By applying Glauber theory we calculate the mean number of *events* per unit of rapidity:

$$\frac{dN^f}{dy}=T_{AA}(b)\,\frac{d\sigma^f_{\rm hard}}{dy}, \tag{8}$$

where the nuclear overlap function $T_{AA}(b)$ for central events is given by $T_{AA}(0)\approx A^2/\pi R_A^2$. For the nuclei in our calculation this gives $T_{\rm AuAu}(0)=29/{\rm mb}$ and $T_{\rm PbPb}(0)=32/{\rm mb}$. Again it should be emphasized that dN^f/dy gives the number of collisions and that the total number of partons is twice as high in a $2\to 2$ process. The necessary volume, needed to derive the densities from the absolute numbers, is calculated as

$$V_i=\pi R_A^2\Delta y/p_0,\quad R_A=A^{1/3}\times 1.1\ \text{fm}. \tag{9}$$

Therefore we get $V_i({\rm Au+Au})=12.9\ {\rm fm}^3$ and $V_i({\rm Pb+Pb})=13.4\ {\rm fm}^3$.

For the energy density at midrapidity we need the first E_T moment:

TABLE IV. $\sigma^g\langle E_T\rangle$ (mb GeV).

Range of y	$gg\to gg$	$gq\to gq + g\bar{q}\to g\bar{q}$	Total
$\lvert y\rvert\leq 0.5$	18.0	8.7	26.7

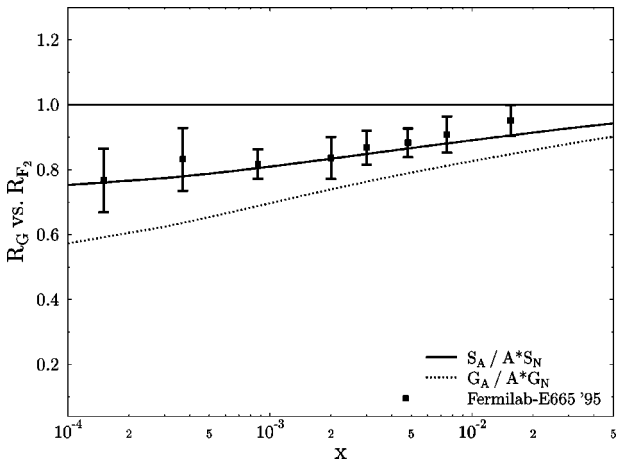

FIG. 2. R_{F_2} vs R_G at $Q^2=4$ GeV^2 for ^{40}Ca.

$$\sigma^f\langle E_T\rangle = \int dE_T \frac{d\sigma^f}{dE_T}\langle E_T\rangle$$

$$= \int dp_T^2 dy\, dy_2 \sum_{ij,kl} x_1 f_i(x_1,Q^2) x_2 f_j(x_2,Q^2)$$

$$\times \left[\delta_{fk} \frac{d\hat{\sigma}^{ij\to kl}}{d\hat{t}}(\hat{t},\hat{u}) + \delta_{fl} \frac{d\hat{\sigma}^{ij\to kl}}{d\hat{t}}(\hat{u},\hat{t}) \right] \frac{1}{1+\delta_{kl}} p_T \epsilon(y). \qquad (10)$$

Here the acceptance function $\epsilon(y)$ is $\epsilon(y)=1$ for $|y|\leqslant 0.5$ and $\epsilon(y)=0$ otherwise.

III. NUCLEAR SHADOWING

In heavy ion collisions one has to account for an effect that does not appear for processes involving two nucleons only: nuclear shadowing. In the lab frame the deep inelastic scattering at small Bjorken x $(x\ll 0.1)$ proceeds via the vector mesons as described in the vector meson dominance model (VMD) where the handbag graph contribution becomes small. In VMD the interaction of the virtual photon with a nucleon or nucleus is described as a two-step process: the photon fluctuation into a $q\bar{q}$ pair (the ρ,ω,ϕ mesons at small Q^2) within the coherence time l_c and a subsequent strong interaction with the target [8]. The coherence time arises in this picture from the longitudinal momentum shift between the photon and the fluctuation: $l_c \approx 1/\Delta k_z$ where $\Delta k_z = k_z^\gamma - k_z^h$. The cross section is

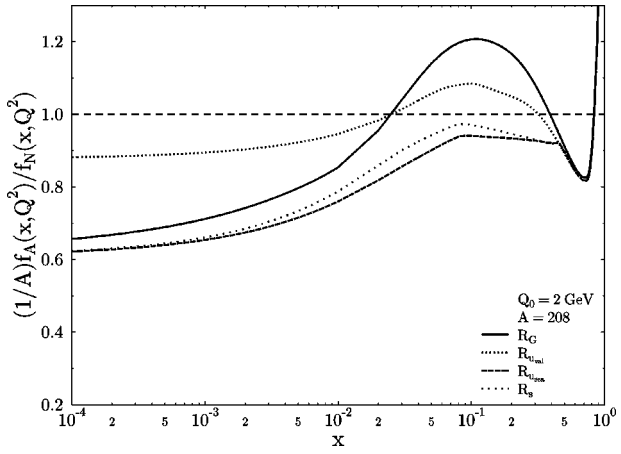

FIG. 3. Shadowed parton distributions as parametrized by Eskola *et al.* in [15]. Note that the gluon shadowing appears to be weaker than quark shadowing and that the onset happens for smaller x.

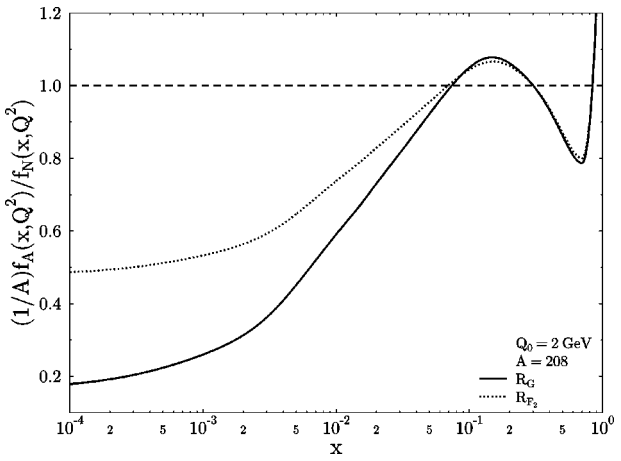

FIG. 4. Our variation of the parametrization given in [16] with much stronger gluon shadowing as found in the VMD calculation in [4]. The stronger shadowing is also motivated by the fact that we calculate central collisions where the shadowing effect is stronger than for b-averaged collisions.

$$\sigma(\gamma^* N) = \int_0^1 dz \int d^2r |\psi(z,r)|^2 \sigma_{q\bar{q}N}(r), \qquad (11)$$

where the Sudakov variable z gives the momentum fraction carried by the quark or the antiquark. The interaction of the fluctuation with the nucleon can be described in the color transparency model as [9]

$$\sigma_{q\bar{q}N} = \frac{\pi^2}{3} r^2 \alpha_s(Q'^2) x' g(x',Q'^2), \qquad (12)$$

where $x' = M_{q\bar{q}}^2/(2m\nu)$, r is the transverse separation of the pair, and $Q'^2 = 4/r^2$. For the interaction of the fluctuation with a nucleus one makes use of Glauber-Gribov multiple-scattering theory [10] where the fluctuation interacts coherently with more than one nucleon in the nucleus when the coherence length exceeds the mean separation between two nucleons:

TABLE V. $\sigma^q\langle E_T\rangle$ (mb GeV).

Range of y	$gq\to gq$	$qq\to qq$	$gg\to q\bar{q}$	$q\bar{q}\to q\bar{q}$	Total
$\lvert y\rvert\leqslant 0.5$	2.1	0.8	0.1	0.2	3.2

TABLE VI. $\sigma^{q}\langle E_T\rangle$ (mb GeV).

Range of y	$g\bar{q}\to g\bar{q}$	$\bar{q}\bar{q}\to\bar{q}\bar{q}$	$gg\to q\bar{q}$	$q\bar{q}\to q\bar{q}$	Total
$\lvert y\rvert\leqslant 0.5$	1.2	0.5	0.1	0.004	1.8

$$\sigma_{q\bar{q}A}=\int d^2b(1-e^{-\sigma_{q\bar{q}N}T_A(b)/2}). \tag{13}$$

When expanding for large nuclei and taking the dominating double-scattering term only one finds

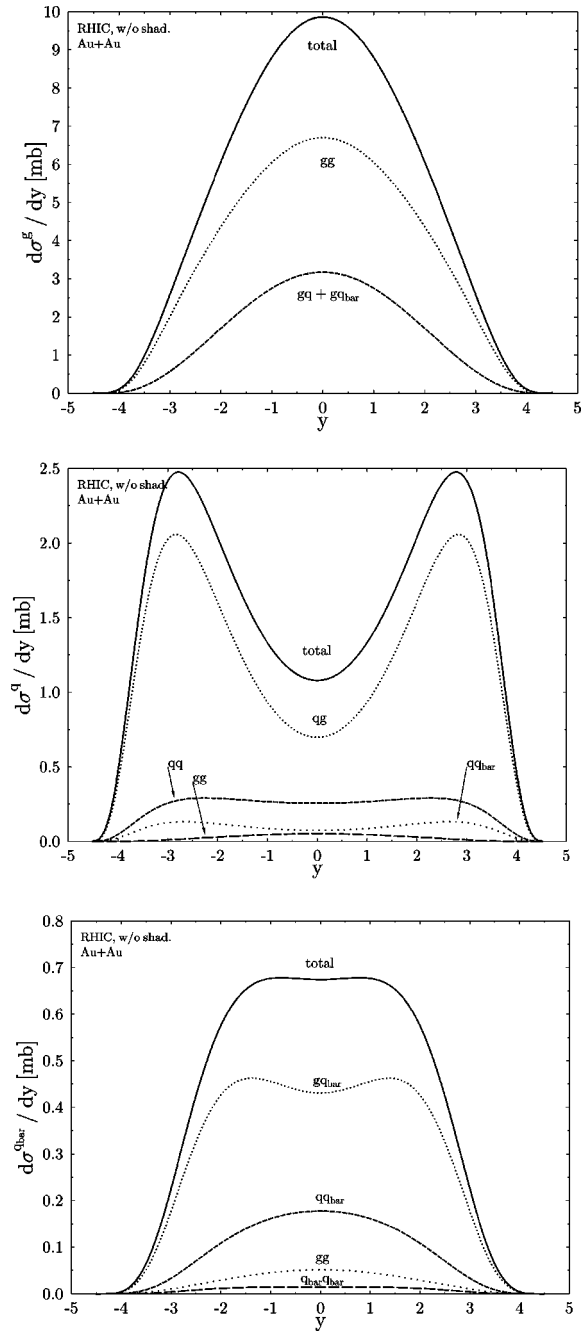

FIG. 5. Unshadowed rapidity distributions of gluons, quarks, and antiquarks.

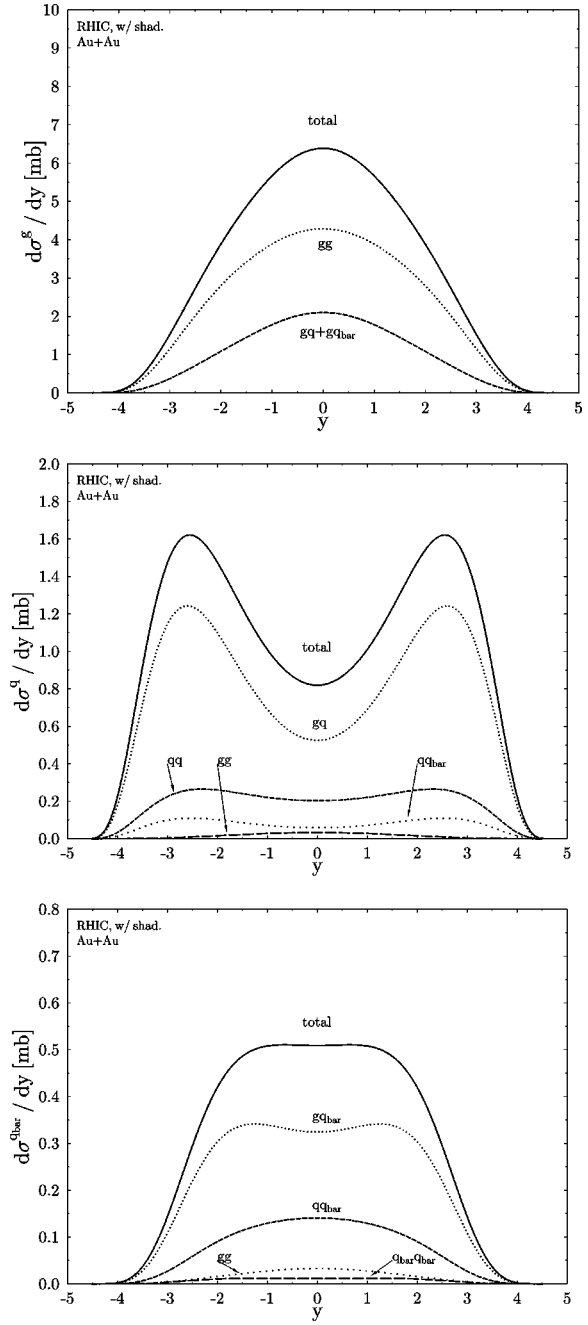

FIG. 6. Rapidity distributions of gluons, quarks, and antiquarks with our modified shadowing parametrization shown in Fig. 4.

$$\sigma_{hA}=A\sigma_{hN}\left[1-A^{1/3}\frac{\sigma_{hN}}{8\pi a^2}+\cdots\right], \tag{14}$$

with $a=1.1$ fm. Figures 1 and 2 show the results for ^{207}Pb and ^{40}Ca (for further details see [4]).

TABLE VII. $\int dy\, dN^g/dy$ for $\sqrt{s}=200A$ GeV.

Range of y	$gg\to gg$	$gq\to gq+g\bar{q}\to g\bar{q}$	Total
All y	581.5	249.4	830.9
$\lvert y\rvert\leqslant 0.5$	122.6	60.2	182.8

TABLE VIII. $\int dy\, dN^q/dy$ for $\sqrt{s}=200A$ GeV.

Range of y	$gq\to gq$	$qq\to qq$	$gg\to q\bar{q}$	$q\bar{q}\to q\bar{q}$	Total
All y	196.5	48.6	3.6	18.1	266.8
$\lvert y\rvert\leqslant 0.5$	15.9	5.9	0.9	1.7	24.4

A very different scenario is employed in parton-fusion models. Here the process of parton-parton fusion in nuclei can be understood as an overlapping of quarks and gluons that yields a reduction of number densities at small x and a creation of antishadowing for momentum conservation at larger x [11]. The onset of this fusion process can be estimated to start at values of the momentum fraction where the longitudinal wavelength $(1/xP)$ of a parton exceeds the size of a nucleon (or the internucleon distance) inside the Lorentz contracted nucleus: $1/xP\approx 2R_n M_n/P$, corresponding to a value $x\approx 0.1$. Originally the idea of parton fusion was proposed in [12] and later proven in [13] to appear when the total transverse size $1/Q$ of the partons in a nucleon becomes larger than the proton radius to yield a transverse overlapping within a unit of rapidity, $xG(x)\geqslant Q^2R^2$. The usual gluon distribution in the nucleon on the light cone in light-cone gauge $(n\cdot A=A^+=0)$ is given by

$$xG(x)=-(n^-)^2\int\frac{d\lambda}{2\pi}\langle P|F^{+\mu}(0)F^+_\mu(\lambda n)|P\rangle. \quad (15)$$

The recombination is then described as the fusion of two gluon ladders into a single vertex. One finally arrives at a modified Altarelli-Parisi equation where the fusion correction enters as a twist four light cone correlator. Typically the fusion correction in the free nucleon turns out to be significant only for unusually small values of x or Q^2. As shown in [14] the situation changes dramatically in heavy nuclei. Here the strength of the fusion for ladders coming from independent constituents increases and is of the same order as the fusion from nonindependent constituents. Therefore, parton recombination is strongly increased in heavy nuclei of $A\sim 200$.

Unfortunately the different models do not give the same results for the ratio $R_G(x,Q^2)$. We will, therefore, use two versions of parametrizations to investigate the effects of shadowing on the relevant variables. On the one hand, we use a Q^2-dependent version of Eskola, Kolhinen, Salgado, and Ruuskanen, often referred to as ''98 shadowing'' (see Fig. 3), that tries to avoid any model dependence by using sum rules for baryon number and momentum [15] and, on the other hand, we use a modified version of a Q^2-independent parametrization (see Fig. 4) given in [16] which employs a much stronger gluon shadowing in accordance with the results of [4]. Especially for RHIC, where the lower bound for the momentum fraction at midrapidity for $p_T=p_0=2$ GeV is given by $x=2p_T/\sqrt{s}=0.02$, the onset of the gluon shadowing, i.e., the transition region between shadowing and antishadowing, is of great importance.

TABLE IX. $\int dy\, dN^{\bar{q}}/dy$ for $\sqrt{s}=200A$ GeV.

Range of y	$g\bar{q}\to g\bar{q}$	$q\bar{q}\to q\bar{q}$	$gg\to q\bar{q}$	$\bar{q}\bar{q}\to\bar{q}\bar{q}$	Total
All y	52.9	18.1	3.6	1.8	76.4
$\lvert y\rvert\leqslant 0.5$	9.4	4.1	0.9	0.3	14.7

TABLE X. $\sigma^g\langle E_T\rangle$ (mb GeV).

Range of y	$gg\to gg$	$gq\to gq+g\bar{q}\to g\bar{q}$	Total
$\lvert y\rvert\leqslant 0.5$	11.9	5.9	17.8

In [15] the onset of gluon shadowing $(R_G=1)$ is chosen at $x\approx 0.029$ for $Q=2$ GeV motivated by the results found in [17] where the connection between the gluon distribution and the Q^2 dependence of F_2 via the DGLAP equations was employed:

$$\frac{\partial F_2}{\partial\ln Q^2}\sim\sum_i e_i^2 xG(2x,Q^2). \quad (16)$$

By using the NMC data [18] on deep inelastic scattering on a combination of Sn and C targets the ratio $G^{\mathrm{Sn}}(x)/G^{\mathrm{C}}(x)$ was derived in the range $0.011\leqslant x\leqslant 0.18$. The crossover point can, despite the large errorbars, be guessed to be $x\approx 0.03$. However, one should add here that the situation for $R_G^{\mathrm{Pb}}=xG^{\mathrm{Pb}}(x)/xG^N(x)$ can look rather different. Since this question of the onset of gluon shadowing is not yet settled we chose the same onset for quark and gluon shadowing in our modified parametrization to investigate the relevance of this point. We fixed $R_{F_2}=R_G=1$ at $x\approx 0.07$. In VMD as well as in parton fusion models the onset is treated on an equal footing: for the coherent scattering processes in VMD it should make no difference (at least for the onset) whether a $q\bar{q}$ or a gg pair scatters from more than one nucleon at $l_c\geqslant r_{NN}$. In the parton fusion model one treats the leaking out of the partons equally for sea quarks and for gluons since for both sea quarks and for gluons one has a spatial extent of $1/xP$ in the longitudinal direction and therefore, the onset for R_G and R_{F_2} is essentially the same in this model.

IV. RESULTS

In the following we will give the results for the different parton species $f=g,q,\bar{q}$ at RHIC and LHC including the different shadowing parametrizations or no shadowing, respectively. The results for the number of partons $\int dN^f/dy$ can easily be derived from $\int dy\, d\sigma^f/dy$ by the relation $dN^f/dy=T_{AA}(0)d\sigma^f/dy$. All results include a K factor of K=2.5 for RHIC and $K=1.5$ for LHC. On the one hand, we give the results for the whole y range and, on the other hand, we give the result for the central rapidity region which is of

TABLE XI. $\sigma^q\langle E_T\rangle$ (mb GeV).

Range of y	$gq\to gq$	$qq\to qq$	$gg\to q\bar{q}$	$q\bar{q}\to q\bar{q}$	Total
$\lvert y\rvert\leqslant 0.5$	0.6	0.3	0.04	0.1	1.0

TABLE XII. $\sigma^{\bar{q}}\langle E_T\rangle$ (mb GeV).

Range of y	$gq\to gq$	$qq\to qq$	$gg\to q\bar{q}$	$q\bar{q}\to q\bar{q}$	Total
$\lvert y\rvert\leqslant 0.5$	0.4	0.01	0.04	0.2	0.7

special interest, not only from the experimental setup point of view but also since it is the region where the highest parton densities and the strongest shadowing effects are expected.

Let us start by giving the results without shadowing corrections for RHIC. Tables I, II, and III give the unshadowed multiplicities integrated over the whole rapidity range and over the central region, respectively. Tables IV–VI give the first E_T moments for the respective parton species. The rapidity distributions for the cross sections are depicted in Fig. 5.

For the strong gluon shadowing shown in Fig. 4 one finds the multiplicities (see Tables VII, VIII, and IX) for the different parton species (the rapidity distributions are shown in Fig. 6) The first E_T moments for the reactions including our modified strong gluon shadowing are given in Tables X, XI, and XII. We also calculated the multiplicities and first E_T moments by employing the newest available shadowing parametrization of Eskola *et al.* of Ref. [15] shown in Fig. 3. As emphasized above one should note that the shadowing of gluons in this parametrization is smaller than the quark shadowing since we tried to stay away from any model dependence and just stick to sum rules expressing the momentum and baryon number conservation but still assuming that at small x ($x\approx 10^{-4}$) the gluon ratio should coincide with the sea quark ratio. By employing this version we find the results listed in Tables XIII–XV and shown in Fig. 7.

In Fig. 8 we directly compared the strong gluon shadowed distributions (left figure) with the unshadowed one. The same was done for the comparison of the Q^2-dependent 98 shadowing version [15] with the unshadowed one (right figure). The solid lines give the total contribution, the dotted ones the contribution from the gg subprocess and the dashed lines give the $gq+g\bar{q}$ contribution. The thick lines denote the unshadowed distributions and the thin ones the two shadowed ones. Note that due to the onset of gluon shadowing in the 98 version at such small values of x, one even gets an enhancement for the $gg\to gg$ subprocess at RHIC. We also calculated the p_T distribution without and with the two shadowing versions at midrapidity (Fig. 9). Unlike the strong shadowing case the crossover point of the curves already happens at $p_T\approx 2.5$ GeV for the 98 gluon shadowing version which immediately explains the enhancement in the rapidity distribution. For the first E_T moment of the transverse energy we find with the shadowing parametrization of Eskola *et al.* the results shown in Table XVI. From the results in Tables XVII and XVIII, we can calculate the total transverse energy $E_T=\sigma\langle E_T\rangle T_{AA}(0)$ carried by the partons, the number and energy densities n_f and ε_f, and also derive the initial temperature T_i if we assume the behavior of an ideal gas of partons. To do so we need the initial volume. With $R_A=A^{1/3}\times 1.1$ fm, $T_{\mathrm{AuAu}}(0)=29$/mb, and $R_{\mathrm{Au}}=6.4$ fm we find $V_i=\pi R_A^2\Delta y\,\tau=12.9$ fm^3.

TABLE XIII. $\int dy\, dN^g/dy$ for $\sqrt{s}=200A$ GeV.

Range of y	$gg\to gg$	$gq\to gq+g\bar{q}\to g\bar{q}$	Total
All y	969.5	350.2	1319.7
$\lvert y\rvert\leqslant 0.5$	201.8	81.9	283.7

TABLE XIV. $\int dy\, dN^q/dy$ for $\sqrt{s}=200A$ GeV.

Range of y	$gq\to gq$	$qq\to qq$	$gg\to q\bar{q}$	$q\bar{q}\to q\bar{q}$	Total
All y	282.8	50.8	65.3	18.9	417.8
$\lvert y\rvert\leqslant 0.5$	19.6	6.3	1.5	1.7	29.1

Therefore, at RHIC without any shadowing and with $K=2.5$ we have at midrapidity a total number of 284 gluons, 32 quarks, and 20 antiquarks. These carry a transverse energy of 774 GeV (gluons), 93 GeV (quarks), and 55 GeV (antiquarks). It is then straight forward to derive the number densities by dividing by the initial volume to yield $n_g=22$ fm^{-3}, $n_q=2.5$ fm^{-3}, $n_{\bar{q}}=1.5$ fm^{-3}. The energy densities can be derived in an analogous way to give: $\varepsilon_g=60$ GeV/fm^{-3}, $\varepsilon_q=7.2$ GeV/fm^{-3}, and $\varepsilon_{\bar{q}}=4.3$ GeV/fm^{-3}. If we assume total equilibrium we can derive the initial temperature from these numbers as

$$\varepsilon^{\mathrm{ideal}}=16\pi^2\frac{3}{90}T_{\mathrm{eq}}^4. \tag{17}$$

At this point some comments are appropriate: one could wonder whether the system can be in equilibrium since one has only hard $2\to 2$ parton scatterings in this Glauber approach. Also one often assumes global equilibrium to be established after, say 1 fm/c. Now here we are mainly interested in local equilibrium as it is required, for example, for hydrodynamical calculations. The equilibration of partons in a local cell happens to be much faster for the following reasons. The high Q^2 hard scatterings among the partons are absolutely unimportant for the equipartition of longitudinal and transverse degrees of freedom. It is the soft interactions that are responsible for this feature and there is a huge resource of soft partons available in the nucleons, even when assuming the parton distributions to be shadowed in heavy nuclei. The link to the short equilibration time is the fact that even though the nucleus is Lorentz contracted to $L/\cosh y$, the partons obey the uncertainty principle and are, therefore, smeared out to distances $1/xP$ in the infinite momentum frame and so the major part of the partons is *outside* the Lorentz contracted disk. Based on some basic principles and by using the Fokker-Planck equation [1,19] the time it takes to establish local equilibrium in a cell was estimated to have

TABLE XV. $\int dy\, dN^{\bar{q}}/dy$ for $\sqrt{s}=200A$ GeV.

Range of y	$g\bar{q}\to g\bar{q}$	$q\bar{q}\to q\bar{q}$	$gg\to q\bar{q}$	$\bar{q}\bar{q}\to\bar{q}\bar{q}$	Total
All y	66.8	18.7	65.3	16.7	167.5
$\lvert y\rvert\leqslant 0.5$	10.9	4.1	1.5	0.3	16.9

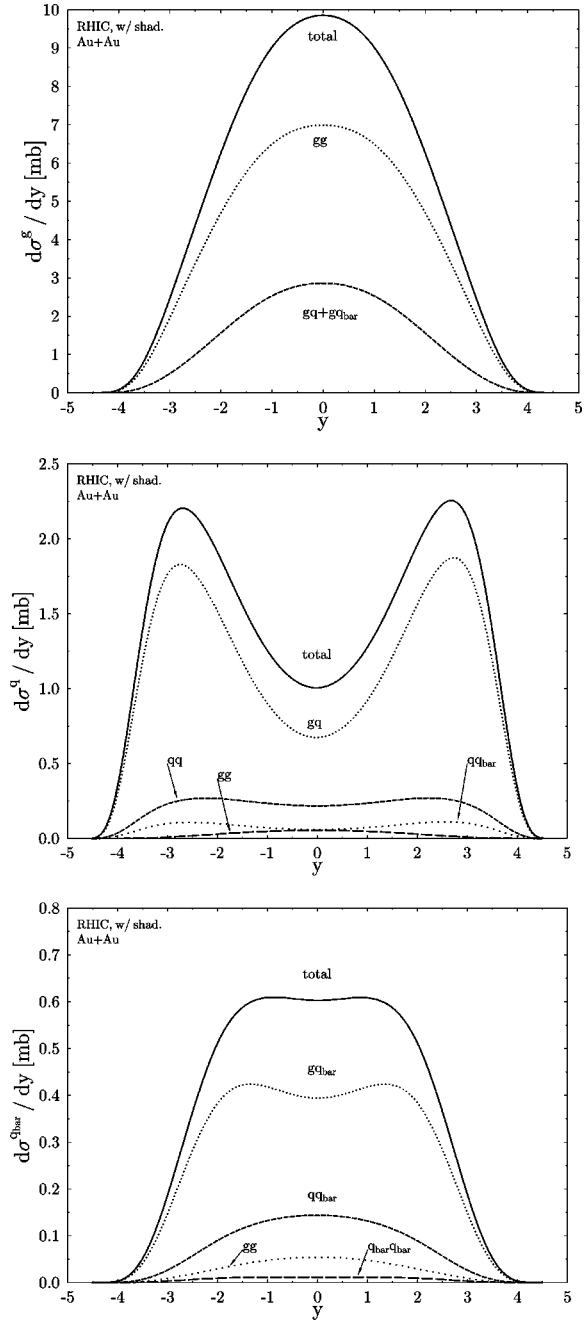

FIG. 7. Rapidity distributions of gluons, quarks, and antiquarks with the 98 version of the shadowing parametrization shown in Fig. 3.

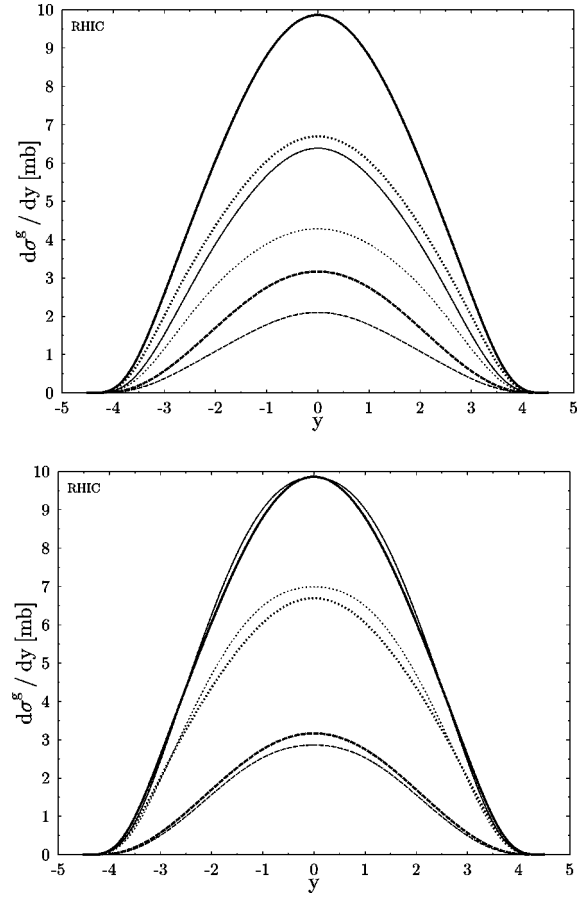

FIG. 8. Comparison of the rapidity distributions with strong gluon shadowing (top figure) and weak shadowing (bottom figure) to unshadowed distribution for RHIC (see text).

a lower bound of $\tau_0 \approx 0.15$ fm/c. As noted above we introduced a lower momentum cutoff $p_0 = 2$ GeV corresponding to a proper time of about 0.1 fm/c. So, therefore, we may not be far from local equilibration and the calculation of the initial temperature from the initial energy density could be rather justified. However, we should emphasize that the results for the energy and number densities and for the initial temperatures are only due to the hard scatterings with $p_T \geqslant 2$ GeV and contributions from soft parton production at $p_T < 2$ GeV are not entering our results.

For the temperature we take into account only the gluons due to their large multiplicity and energy density that dominates the respective values for the quarks. We then find $T_i = 549.5$ MeV for RHIC. If we neglect all higher orders, i.e., take a K factor of $K = 1$ (which of course is wrong, but it is instructive to see the impact on T_i), we get $T_i^{K=1} = 437$ MeV. The same quantities were then calculated for the two different shadowing scenarios. For the calculations employing the strong gluon shadowing we found that there are 183 gluons, 25 quarks, and 15 antiquarks carrying transverse energies of 516 GeV (gluons), 29 GeV (quarks), and 17 GeV (antiquarks). The resulting number and energy densities are found to be $n_g = 14$ fm^{-3}, $n_q = 1.9$ fm^{-3}, $n_{\bar{q}}$

TABLE XVI. $\sigma^g \langle E_T \rangle$ (mb GeV).

Range of y	$gg \to gg$	$gq \to gq + g\bar{q} \to g\bar{q}$	Total
$\lvert y \rvert \leqslant 0.5$	19.2	8.1	27.3

TABLE XVII. $\sigma^q \langle E_T \rangle$ (mb GeV).

Range of y	$gq \to gq$	$qq \to qq$	$gg \to q\bar{q}$	$q\bar{q} \to q\bar{q}$	Total
$\lvert y \rvert \leqslant 0.5$	2.0	0.7	0.2	0.02	2.9

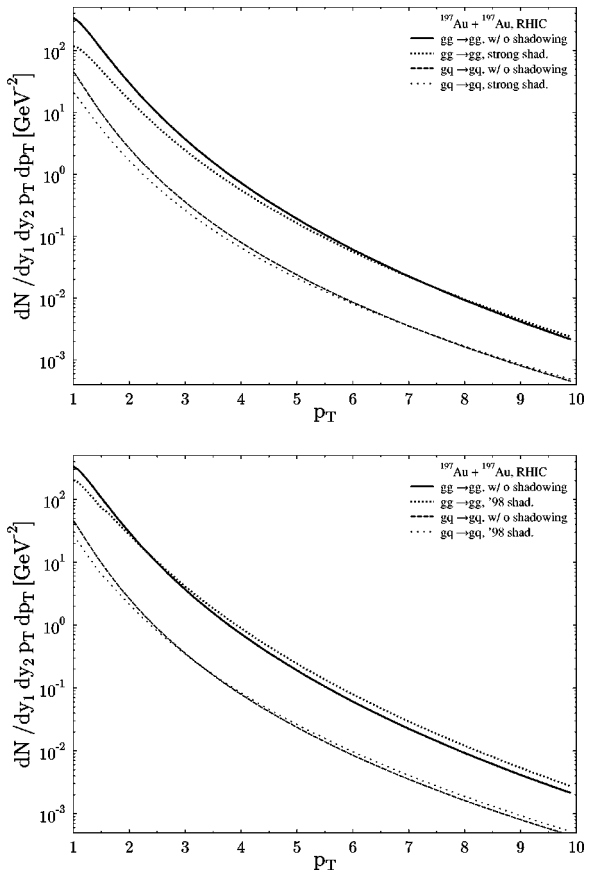

FIG. 9. p_T distributions for the two shadowing parametrizations at midrapidity.

$=1.2$ fm^{-3}, $\varepsilon_g=40$ GeV/fm^{-3}, $\varepsilon_q=2.3$ GeV/fm^{-3}, and $\varepsilon_{\bar{q}}=1.3$ GeV/fm^{-3}. When we calculate the initial temperature for an ideal parton gas from these numbers we find that the initial temperature decreases due to the reduced number and energy densities having their origin in the shadowing of the parton distributions. We find $T_{i,\mathrm{shad}}=496.5$ MeV for a K factor of 2.5 and when neglecting all higher-order contributions we derive $T^{K=1}_{i,\mathrm{shad}}=394.9$ MeV. So what we learn here is the following: due to the reduced number of partons involved in the hard processes a reduction in the number densities and therefore in the energy densities entering the formula for the temperature of a thermalized parton gas results. One should note that the onset of shadowing in our modified shadowing parametrization was chosen to be the same for quarks and gluons in accordance with the onset of coherent scattering of a quark antiquark or gluon gluon pair, respectively, off a nucleus. Now, in the second shadowing parametrization we employed [15], one finds that the onset of shadowing for gluons starts at smaller momentum fractions from $xG^{Sn}(x)/xG^{C}(x)$ data. With a momentum cutoff $p_0=2$ GeV the momentum fractions involved in processes at midrapidity are bound from below at $x=0.02$. Therefore, one is right on the edge of the onset of shadowing of the parametrizations. Also one should expect the very interesting case that one is on the edge of the antishadowing region for gluons in the 98 parametrization of Eskola *et al.* but not so for the parametrization employing the strong gluon shadowing. This behavior is immediately reflected in the number and energy densities. We found that for this specific shadowing parametrization one has 284 gluons, 29 quarks, and 17 antiquarks carrying transverse energies of 790 GeV (gluons), 83 GeV (quarks), and 50 GeV (antiquarks). We found the following densities: $n_g=22$ fm^{-3}, $n_q=2.2$ fm^{-3}, $n_{\bar{q}}=1.3$ fm^{-3}, $\varepsilon_g=61.2$ GeV/fm^{-3}, $\varepsilon_q=6.4$ GeV/fm^{-3}, and $\varepsilon_{\bar{q}}=3.9$ GeV/fm^{-3}. These numbers result in an initial temperature of $T_{i,\mathrm{shad}}=552.3$ MeV and $T^{K=1}_{i,\mathrm{shad}}=439.2$ MeV, respectively.

We also went through the same program to investigate the impact of the different shadowing parametrizations at the higher LHC energy of $\sqrt{s}=5.5$ TeV. We here used the newer parton distributions of CTEQ4L since the involved momentum fractions are so small that any new information at small x are valuable. When comparing GRV '94 and CTEQ4L one finds a difference of about a factor of 2 at $x\approx10^{-5}$. At LHC energies the effect of shadowing should be much more relevant than at RHIC due to the region of smaller x that gets probed. Because of the strong dominance of the gluon component in the nucleon we restricted ourself to the calculation of σ^g, $\overline{N^g}$ and, therefore, on the transverse energy and temperature produced by the final state gluons only. We show unshadowed results in Tables XIX and XX. The rapidity distributions for unshadowed and shadowed gluons at LHC are depicted in Fig. 10. For the strong gluon shadowing we show the results in Tables XXI and XXII. With the weaker gluon shadowing one finds that shown in Tables XXIII and XXIV. A direct comparison between the results for shadowed and unshadowed parton distribution functions is shown in Fig. 11 and the p_T distributions for LHC are shown in Fig. 12.

Therefore, we find the following numbers at LHC: for unshadowed parton distributions one has at midrapidity 4845 gluons that carry a transverse energy of 16.4 TeV. The number density thus is $n_g=363$ fm^{-3} and the energy density is

TABLE XVIII. $\sigma^{\bar{q}}\langle E_T$ (mb GeV).

Range of y	$g\bar{q}\to g\bar{q}$	$\bar{q}\bar{q}\to\bar{q}\bar{q}$	$gg\to q\bar{q}$	$q\bar{q}\to q\bar{q}$	Total
$\lvert y\rvert\leqslant0.5$	1.1	0.03	0.1	0.4	1.6

TABLE XIX. $\int dy\, dN^g/dy$ for $\sqrt{s}=5.5A$ TeV.

Range of y	$gg\to gg$	$gq\to gq+g\bar{q}\to g\bar{q}$	Total
All y	36822.7	6006.1	42828.8
$\lvert y\rvert\leqslant0.5$	4137.6	707.2	4844.8

TABLE XX. $\sigma^g\langle E_T\rangle$ (mb GeV).

Range of y	$gg\to gg$	$gq\to gq+g\bar{q}\to g\bar{q}$	Total
$\lvert y\rvert\leqslant0.5$	438.1	74.9	513.0

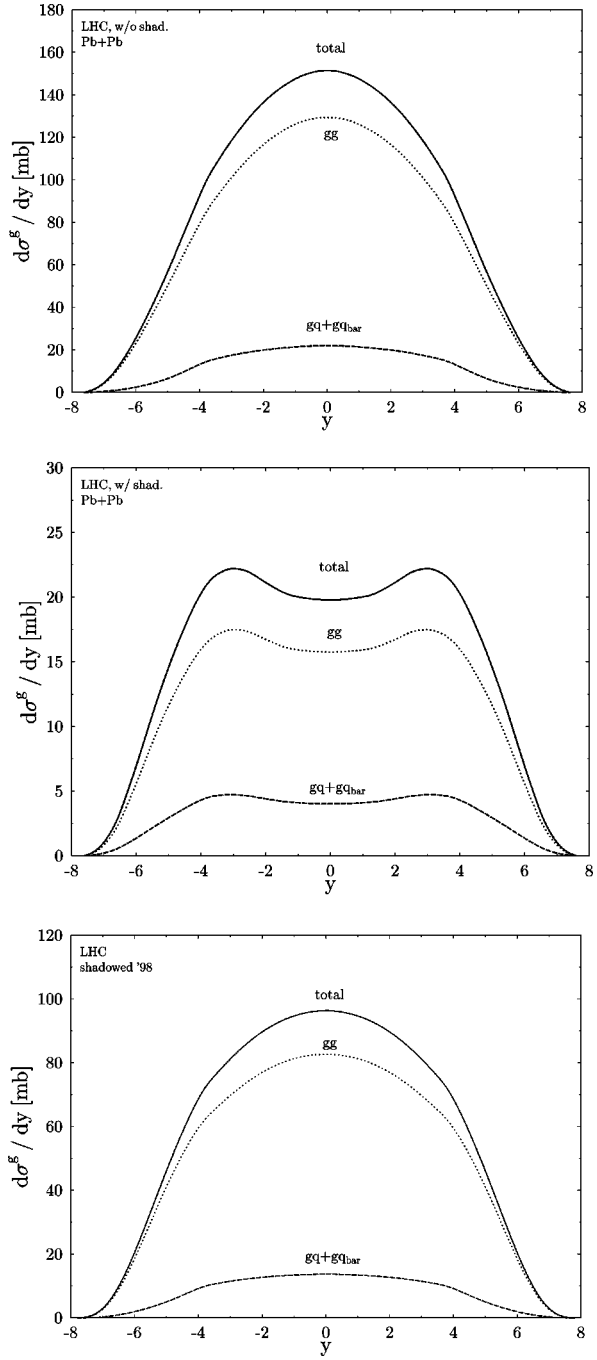

FIG. 10. Rapidity distributions of unshadowed (upper figure) and shadowed gluons (lower two figures) at LHC. The figure in the middle was derived by employing the strong gluon shadowing, whereas the bottom figure employed the Q^2-dependent 98 version. Note the change in shape when the strong gluon shadowing is employed.

TABLE XXI. $\int dy\, dN^g/dy$ for $\sqrt{s}=5.5A$ TeV.

Range of y	$gg\to gg$	$gq\to gq + g\bar{q}\to g\bar{q}$	Total
All y	5968.9	1558.7	7527.6
$\lvert y\rvert\leqslant 0.5$	504.9	129.3	634.2

TABLE XXII. $\sigma^g\langle E_T\rangle$ (mb GeV).

Range of y	$gg\to gg$	$gq\to gq + g\bar{q}\to g\bar{q}$	Total
$\lvert y\rvert\leqslant 0.5$	48.2	12.2	60.4

given by $\varepsilon_g=1229.7$ GeV/fm^{-3}. The initial temperature of an ideal gas derived with these numbers is $T_i=1169$ MeV and $T_i^{K=1.0}=1056.5$ MeV for $K=1$. With the strong gluon shadowing we find 634 gluons carrying a transverse energy of 1.9 TeV. We, therefore, have $n_g=47.5$ fm^{-3} and $\varepsilon_g=144.8$ GeV/fm^{-3} resulting in $T_i=684.9$ MeV for K=1.5 and $T_i^{K=1.0}=618.9$ MeV. With the shadowing version of [15] we find 3082 gluons which carry a total transverse energy of 9.2 TeV, $n_g=230.9$ fm^{-3}, and $\varepsilon_g=678.6$ GeV/fm^{-3} which results in a temperature $T_i=1011.1$ MeV for $K=1.5$ and $T_i^{K=1.0}=913.6$ MeV for $K=1$.

V. ENTROPY PRODUCTION AND π MULTIPLICITIES

As is known, total entropy and entropy density, respectively, play a very important role in the formation of a quark-gluon plasma. Total entropy reaches its final value when the system equilibrates and can, if assuming an adiabatical further evolution, be related to the effective number of degrees of freedom in the quark-gluon and in a pure pion plasma via [20,21]

$$r=\frac{s^{\pi}(T_c)}{s^{qg}(T_c)}\approx 0.7\pm 0.2, \tag{18}$$

where s^{π} and s^{qg} are the entropy densities in the pion and quark-gluon plasma. The total entropy can then be related to the pion multiplicity as

$$\frac{dS}{dy}=c^{qg}\left(\frac{dN^{qg}}{dy}\right)_{b=0}\approx\frac{c^{\pi}}{r}\left(\frac{dN^{\pi}}{dy}\right)_{b=0}, \tag{19}$$

where $c^{qg}=4.02$ for $N_f=4$ and $c^{\pi}\approx 3.6$.

A note on the separation between hard and soft processes is appropriate at this point. As emphasized above we introduced a cutoff at $p_0=2$ GeV to ensure the applicability of perturbative QCD. Nevertheless there is always a soft component contributing to the production of transverse energy neglected in our studies so far. In [7] it was shown that with $p_0=2$ GeV at SPS the hard partons only carry about 4% of

TABLE XXIII. $\int dy\, dN^g/dy$ for $\sqrt{s}=5.5A$ TeV.

Range of y	$gg\to gg$	$gq\to gq + g\bar{q}\to g\bar{q}$	Total
All y	24919.1	3867.8	28786.9
$\lvert y\rvert\leqslant 0.5$	2643.2	438.4	3081.6

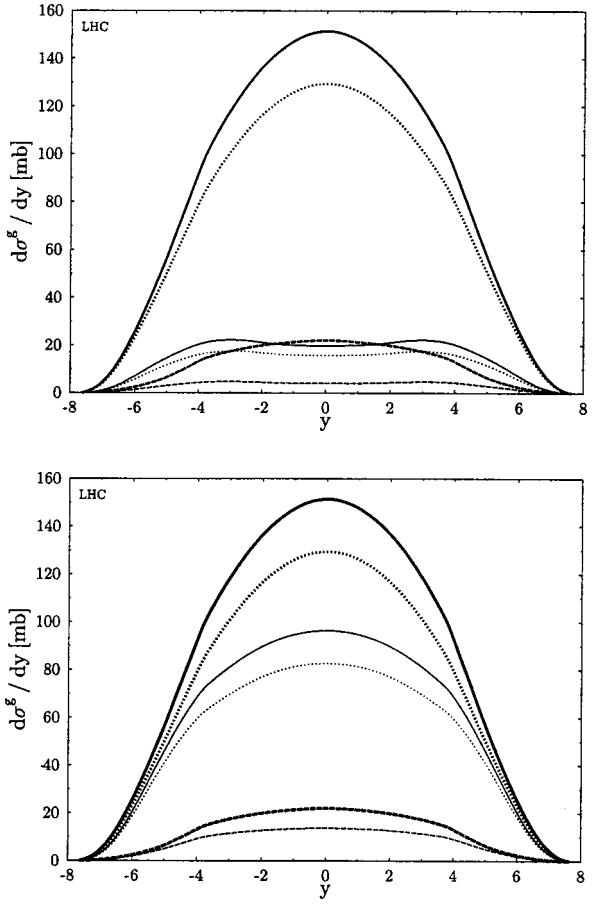

FIG. 11. Comparison of the rapidity distributions with strong (top figure) and weak gluon shadowing (bottom figure) to unshadowed distribution for LHC. The solid lines give the total contribution, the dotted ones depict the $gg \to gg$ process and the dashed ones stand for the $gq \to gq + g\bar{q} \to g\bar{q}$ processes. The thick lines again give the unshadowed results.

the total transverse energy E_T. At RHIC energies they carry $\approx 50\%$ and for $\sqrt{s} = 2$ TeV the hard partons already carry $\approx 80\%$ of the total transverse energy. Since we here solely want to investigate the role of shadowing in hard reactions we will not calculate the pion multiplicity for RHIC where the soft contribution still is significant but restrict ourselves to the pion number at $y \approx 0$ for LHC energies.

If we employ the numbers for the entropy densities in the different plasmas and use our findings on the contributions of shadowing to the number of minijets we find that at $y = 0$ one has

$$\left(\frac{dN^\pi}{dy}\right)_{b=0} \approx 3786,$$

TABLE XXIV. $\sigma^g \langle E_T \rangle$ (mb GeV).

Range of y	$gg \to gg$	$gq \to gq + g\bar{q} \to g\bar{q}$	Total
$\lvert y \rvert \leqslant 0.5$	245.9	41.0	286.9

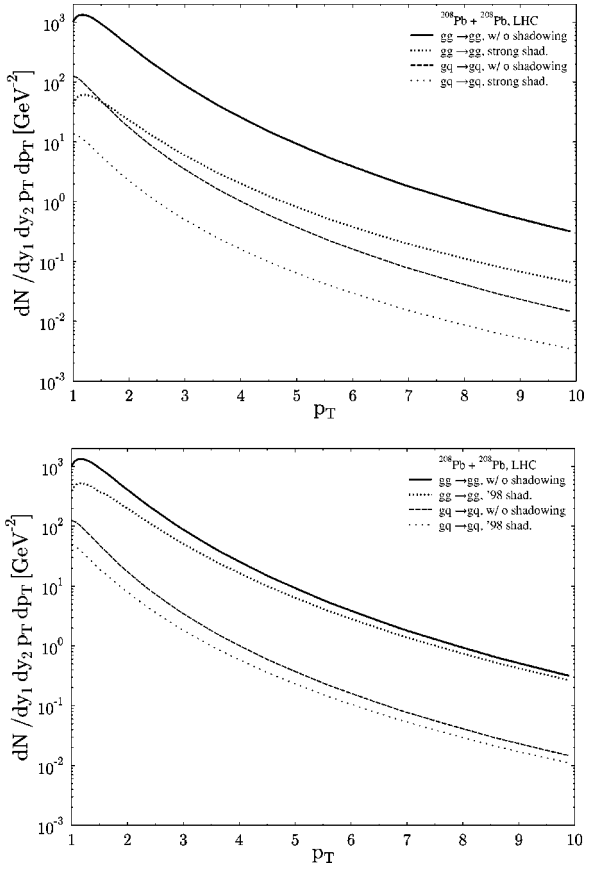

FIG. 12. p_T distributions for the two shadowing parametrizations at midrapidity for LHC.

$$\left(\frac{dN^\pi}{dy}\right)_{b=0} \approx 2413, \tag{20}$$

$$\left(\frac{dN^\pi}{dy}\right)_{b=0} \approx 330,$$

when employing no shadowing, the 98 version of Eskola *et al.*, and the strong gluon shadowing parametrization.

VI. CONCLUSIONS

In this paper we investigated the influence of nuclear shadowing on rapidity spectra, transverse energy production and on macroscopic quantities such as the initial temperature. We employed two different versions of parametrizations for the shadowing: one with a strong initial gluon shadowing and a model independent one recently published by Eskola *et al.* [15]. We found that the latter one gives an enhancement of minijet production at RHIC in contrast to the other case were a reduction to $\approx 65\%$ results. This difference directly manifests itself in the initial temperature T_i which happens to be smaller only for the strong gluon shadowing. At LHC the situation changes since there also the weakly shadowed gluons finally result in lower spectra and T_i. Since the two shadowing parametrizations differ so drastically one finds a large difference in the results for the num-

ber of minijets at midrapidity: for the strong shadowing one has ≈ 630 gluons whereas for the weaker shadowing one finds ≈ 3000 gluons. Since there are so few gluons for the strong gluon shadowing we find that the initial temperature at LHC is not dramatically higher than at RHIC.

ACKNOWLEDGMENTS

We would like to thank K.J. Eskola for many stimulating discussions on minijet production and nuclear shadowing. This work was supported by BMBF, DFG, and GSI.

[1] R. Hwa and K. Kajantie, Phys. Rev. Lett. **56**, 696 (1986).
[2] UA1 Collaboration, C. Albaja *et al.*, Nucl. Phys. **B309**, 405 (1988).
[3] K.J. Eskola and K. Kajantie, Z. Phys. C **75**, 515 (1997).
[4] N. Hammon, H. Stöcker, and W. Greiner, Phys. Lett. B **448**, 290 (1998).
[5] M. Glück, E. Reya, and A. Vogt, Z. Phys. C **67**, 433 (1995).
[6] H.L. Lai, J. Huston, S. Kuhlmann, F. Olness, J. Owens, D. Soper, W.K. Tung, and H. Weerts, Phys. Rev. D **55**, 1280 (1997).
[7] K.J. Eskola, K. Kajantie, and J. Lindfors, Nucl. Phys. **B323**, 37 (1989).
[8] T. Bauer, R. Spital, D. Yennie, and F. Pipkin, Rev. Mod. Phys. **50**, 260 (1978).
[9] B. Blattel, G. Baym, L. Frankfurt, and M. Strikman, Phys. Rev. Lett. **70**, 896 (1993); L. Frankfurt, G. Miller, and M. Strikman, Phys. Lett. B **304**, 1 (1993).
[10] V. N. Gribov, Zh. Éksp. Teor. Fiz. **57**, 1306 (1970) [Sov. Phys. JETP **30**, 709 (1970)]; R. Glauber, in *Lectures in Theoretical Physics*, edited by W.E. Brittin *et al.* (Interscience Publishers, New York, 1959).
[11] F.E. Close, J. Qiu, and R.G. Roberts, Phys. Rev. D **40**, 2820 (1989).
[12] L. Gribov, E. Levin, and M. Ryskin, Phys. Rep. **100**, 1 (1983).
[13] A.H. Mueller and J. Qiu, Nucl. Phys. **B268**, 427 (1986).
[14] K.J. Eskola, J. Qiu, and X. Wang, Phys. Rev. Lett. **72**, 36 (1994).
[15] K.J. Eskola, V.J. Kolhinen, and C.A. Salgado, JYFL-8/98, US-FT/14-98, hep-ph/9807297; K.J. Eskola, V.J. Kolhinen, and P.V. Ruuskanen, CERN-TH/97-345, JYFL-2/98, hep-ph/9802350.
[16] K.J. Eskola, Nucl. Phys. **B400**, 240 (1993).
[17] T. Gousett and H.J. Pirner, Phys. Lett. B **375**, 349 (1996).
[18] A. Mücklich, Ph.D. thesis, University of Heidelberg, 1995.
[19] R. Hwa, Phys. Rev. D **32**, 637 (1985).
[20] J.D. Bjorken, Phys. Rev. D **27**, 140 (1983).
[21] K. Geiger, Phys. Rev. D **46**, 4986 (1992).